High Mobility and Stability of Thin-Film Transistors Using Silicon-Doped Amorphous Indium Tin Oxide Semiconductors

T. W. Seo, Hyun-Suk Kim, Kwang-Ho Lee, Kwun-Bum Chung & Jin-Seong Park

Journal of Electronic Materials

ISSN 0361-5235
Volume 43
Number 9

Journal of Elec Materi (2014)
43:3177-3183
DOI 10.1007/s11664-014-3211-5

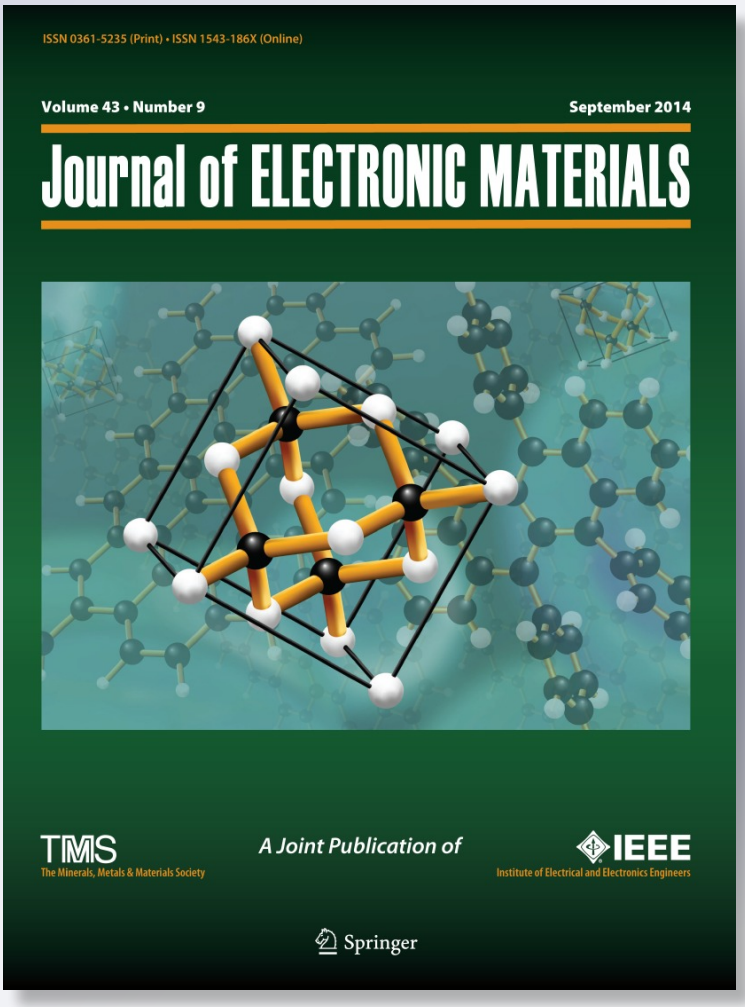

Springer

Journal of ELECTRONIC MATERIALS, Vol. 43, No. 9, 2014
DOI: 10.1007/s11664-014-3211-5

High Mobility and Stability of Thin-Film Transistors Using Silicon-Doped Amorphous Indium Tin Oxide Semiconductors

T. W. SEO,[1] HYUN-SUK KIM,[2,4] KWANG-HO LEE,[1] KWUN-BUM CHUNG,[3,5] and JIN-SEONG PARK[1,6]

1.—Division of Materials Science and Engineering, Hanayng University, 222 Wangsimni-ro, Seoul 133-719, Republic of Korea. 2.—Department of Materials Science and Engineering, Chungnam National University, Daejeon 305-764, Republic of Korea. 3.—Division of Physics and Semiconductor Science, Dongguk University, Seoul 100-715, Republic of Korea. 4.—e-mail: khs3297@cnu.ac.kr. 5.—e-mail: kbchung@dongguk.edu. 6.—e-mail: jsparklime@hanyang.ac.kr

We report the fabrication of high-performance thin-film transistors (TFTs) with an amorphous silicon indium tin oxide (*a*-SITO) channel, which was deposited by cosputtering a silicon dioxide and an indium tin oxide target. The effect of the silicon doping on the device performance and stability of the *a*-SITO TFTs was investigated. The field-effect mobility and stability under positive bias stress of the *a*-SITO TFTs with optimized Si content (0.22 at.% Si) dramatically improved to 28.7 cm^2/Vs and 1.5 V shift of threshold voltage, respectively, compared with the values (0.72 cm^2/Vs and 8.9 V shift) for *a*-SITO TFTs with 4.22 at.% Si. The role of silicon in *a*-SITO TFTs is discussed based on various physical and chemical analyses, including x-ray absorption spectroscopy, x-ray photoelectron spectroscopy, and spectroscopic ellipsometry measurements.

Key words: Silicon-doped InSnO, thin-film transistor, oxide semiconductor, high mobility, stability

INTRODUCTION

Transparent electrodes and TFTs using amorphous oxide semiconductors (AOSs) are emerging as next-generation display solutions because AOSs exhibit high mobility and can be deposited at room temperature.[1–3] In_2O_3-based materials, including InZnO (IZO), InGaZnO (IGZO), and InSnO (ITO) thin films, have attracted much attention as promising candidates for high-performance display applications due to their excellent electrical and optical properties.[4–7] In particular, ITO is the leading candidate for high-performance backplanes as both a semiconductor and electrode layer that offer unique advantages.[8–10] Park et al.[9] recently reported a large field-effect mobility (μ_{FE}) of above 20 cm^2/Vs for ITO TFTs. However, the stability of ITO TFTs needs to be improved for real active-matrix liquid-crystal displays (AMLCDs) or active-matrix organic light-emitting diode (AMOLED) display applications because the threshold voltage is dramatically changed after bias stress testing. It is noted that the stability can be further enhanced by incorporation of suitable (trivalent and/or tetravalent) elements such as gallium (Ga^{3+}), hafnium (Hf^{4+}), zirconium (Zr^{4+}), and silicon (Si^{4+}), which have been used as carrier generation suppressors or stabilizers in IZO semiconductors.[11–14] Although several studies have been performed on ITO TFTs, research on cation doping in the ITO channel has not been reported yet, except for Zn-doped ITO.[15,16]

Herein, we report fabrication of high-performance, high-stability TFTs with an amorphous Si-doped ITO (*a*-SITO) film, which was cosputtered using a SiO_2 and an ITO target to incorporate Si into the ITO matrix as a stabilizer. The silicon content incorporated into the *a*-SITO film was varied by controlling the radiofrequency (rf) power of the SiO_2 target. The effect of the silicon content on

T.W. Seo and Hyun-Suk Kim have contributed equally to this work.
(Received September 16, 2013; accepted April 21, 2014; published online June 14, 2014)

the device characteristics of the fabricated *a*-SITO TFTs was investigated comprehensively based on a variety of physical and chemical analyses. In particular, the physical origins of the change in the electrical properties of *a*-SITO TFTs as a function of the Si concentration are discussed in detail by analyzing the evolution of features of the electronic structure, such as the band alignment and band edge states below the conduction band.

EXPERIMENTAL PROCEDURES

a-SITO films with thickness of 30 nm were grown by cosputtering on heavily doped *p*-type Si wafers with a thermally grown SiO_2 layer (100 nm), using SiO_2 and ITO (In:Sn = 9:1 at.%) targets at room temperature. The cosputtering was carried out at a gas mixing ratio of $O_2/(Ar + O_2) = 0.1$ and a chamber pressure of 1 mTorr. To control the Si content in the *a*-SITO films, the input rf power of the SiO_2 target was varied from 10 W to 40 W, while that of the ITO target was fixed at 60 W. ITO source/drain electrodes (100 nm) were formed by sputtering the ITO target in the same chamber at room temperature. The patterning of the channel and source/drain electrodes was performed using a shadow mask. The fabricated TFTs have an inverted staggered bottom gate structure, as shown in the inset of Fig. 2a, and channel width (W) and length (L) of 1000 μm and 150 μm, respectively. Finally, the sample was subjected to thermal annealing at 150°C for 1 h under vacuum atmosphere. The physical structure was observed by conventional x-ray diffraction (XRD) measurements. To examine the electronic structure near the conduction band of the *a*-SITO films, near-edge x-ray absorption spectroscopy (NEXAS) experiments were performed in total electron yield (TEY) mode at BL-10D of Pohang accelerator laboratory (PAL) in Korea. In addition, changes in band alignment and band edge states below the conduction band were investigated by x-ray photoelectron spectroscopy (XPS) and spectroscopic ellipsometry (SE). The SE measurements were performed using a rotating analyzer system with an auto retarder in the energy range of 0.75 eV to 6.4 eV with incident angles of 65°, 70°, and 75°. The cation atomic ratio and chemical state of the *a*-SITO thin films were analyzed using XPS and Fourier-transform infrared (FT-IR) spectroscopy, respectively. The transfer characteristics of the *a*-SITO TFTs were measured at room temperature using an HP4155B precision semiconductor parameter analyzer.

RESULTS AND DISCUSSION

Figure 1 shows the XRD patterns of the SITO thin films as a function of the SiO_2 rf power. There is no peak originating from any crystalline phase, except for the peak from the Si substrate, which reveals that the SITO films have an amorphous structure, regardless of the SiO_2 rf power (i.e., Si doping concentration) and annealing at 150°C in vacuum. The relative atomic compositions for the *a*-SITO thin films were estimated from the integrated intensity ratio of Si 2*p*, In 3*d*, Sn 3*d*, and O 1*s* core levels of XPS analyses, as summarized in Table I. The oxygen content remained nearly constant at around ~60% as the rf power applied to the SiO_2 target was increased from 10 W to 40 W, but the films exhibited a sharp increase in Si concentration from 0.22 at.% to 4.22 at.%. The FT-IR results (not shown here) revealed that there are Si–O (460 cm^{-1}, Si–O out-of-plane deformation), In–O, and Sn–O bonds in the SITO films, depending on the SiO_2 rf power. However, no significant changes (i.e., in amount or shift) of the Si–O bond signal were found as a function of the SiO_2 power, probably due to insufficient resolution of the FT-IR method. Atomic force microscopy (AFM) analysis also revealed that the Si incorporation did not affect the film surface morphology, with average root-mean-square (RMS) surface roughness of ~0.2 nm.

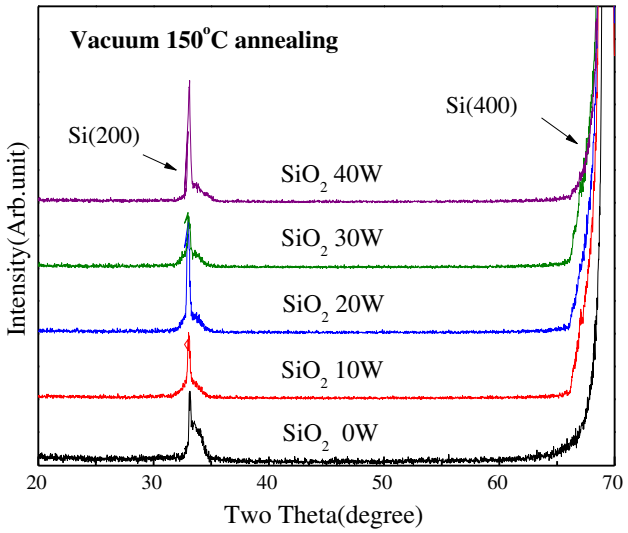

Fig. 1. X-ray diffraction patterns of SITO films deposited on SiO_2/Si substrates using different values of rf power applied to the SiO_2 target. The sharp peak is due to the Si lattice of the substrate.

Figure 2a shows representative transfer characteristics of TFTs with *a*-SITO channels deposited at SiO_2 rf power of 10 W, 20 W, 30 W, and 40 W. The field-effect mobility (μ_{FE}) and threshold voltage (V_{th}) in the saturation region (drain-to-source voltage, V_{DS} = 10 V) were calculated by fitting a straight line to a plot of the square root of I_{DS} (drain-to-source current) versus V_{GS} (gate-to-source voltage), according to the expression for a field-effect transistor.[17] The subthreshold gate swing (S.S.) value was extracted from the linear part of a $\log(I_{DS})$ versus V_{GS} plot.[18] As a reference, pure ITO TFTs normally exhibit conductor-like, rather than semiconducting, characteristics due to the large number of electron carriers (not shown here). A significant improvement in device performance was observed for the TFTs with the *a*-SITO active layer deposited at SiO_2 rf power of 10 W; the detailed

Table I. Oxygen, silicon, indium, and tin contents of *a*-SITO as a function of SiO_2 rf power

Power (W)	Atomic Percent (%)				Parameter				
SiO_2	O 1*s*	Si 2*p*	In 3d^5	Sn 3d^5	V_{th} (V)	μ_{FE} (cm^2/Vs)	S.S. (V/decade)	I_{on}/I_{off}	Hysteresis (V)
10	59.18	0.22	37.47	3.13	−1.17	28.68	0.32	7.48×10^9	2.82
20	60.32	1.8	35.11	2.77	0.1	7.292	0.17	1.85×10^8	3.43
30	59.28	3.43	34.61	2.68	0.26	1.57	0.19	3.90×10^8	4.05
40	60.66	4.22	32.69	2.43	2.09	0.719	0.32	1.05×10^8	4.67

The atomic ratios of the *a*-SITO films were analyzed based on the XPS spectra. TFT parameters include V_{th}, μ_{FE}, S.S., and I_{on}/I_{off} ratio with width/length = 1000 μm/150 μm.

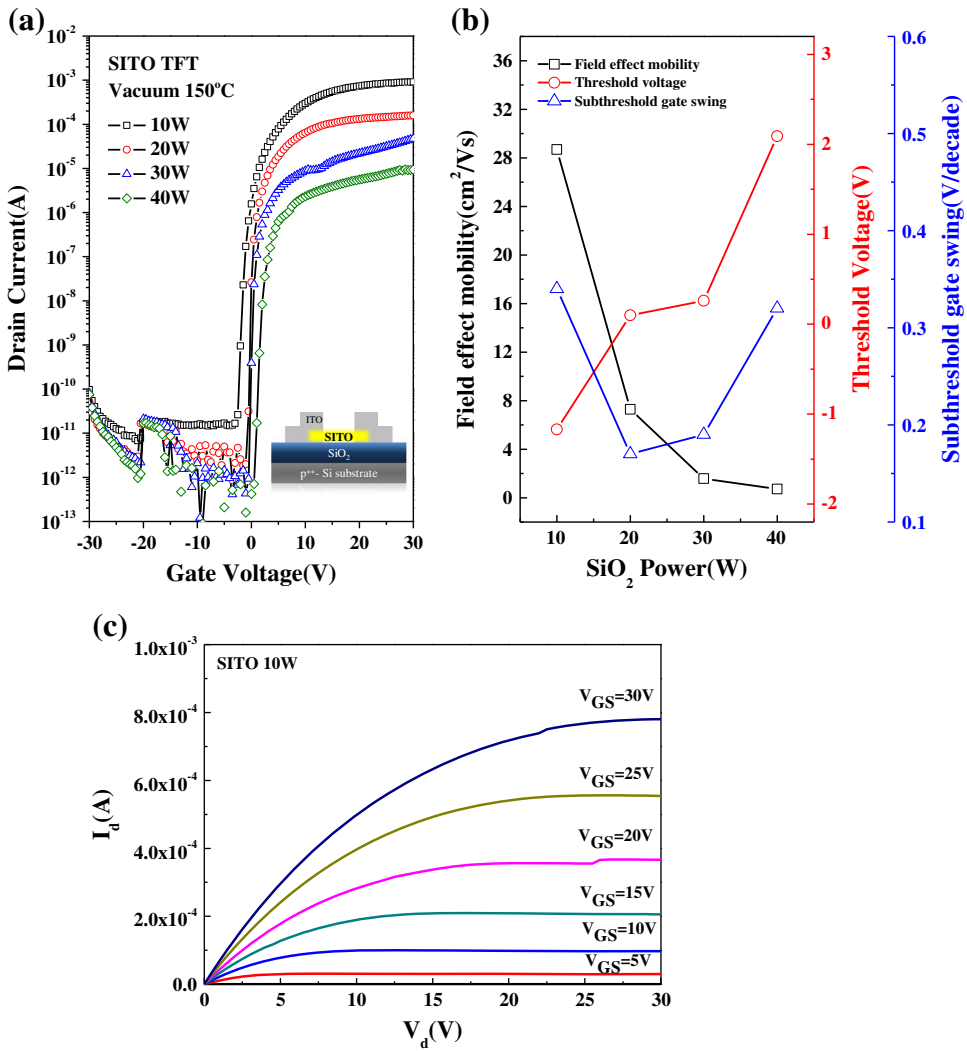

Fig. 2. (a) Transfer characteristics of *a*-SITO TFTs with different values of rf power applied to the SiO_2 target and (b) SiO_2 rf power dependence of extracted electrical parameters such as the field-effect mobility, threshold voltage, and subthreshold swing. The inset of (a) shows a schematic cross-section of the *a*-SITO TFTs, which have an inverted staggered bottom gate structure. (c) Output characteristic of *a*-SITO TFT with SiO_2 target power (10 W).

device parameters are summarized in Table I. Figure 2b shows the SiO_2 rf power dependence of the μ_{FE}, S.S., and V_{th} parameters of the TFTs with cosputtered *a*-SITO films. As the silicon content was increased, the μ_{FE} value of the *a*-SITO TFTs significantly decreased from 28.7 cm^2/Vs (0.22 at.% Si)

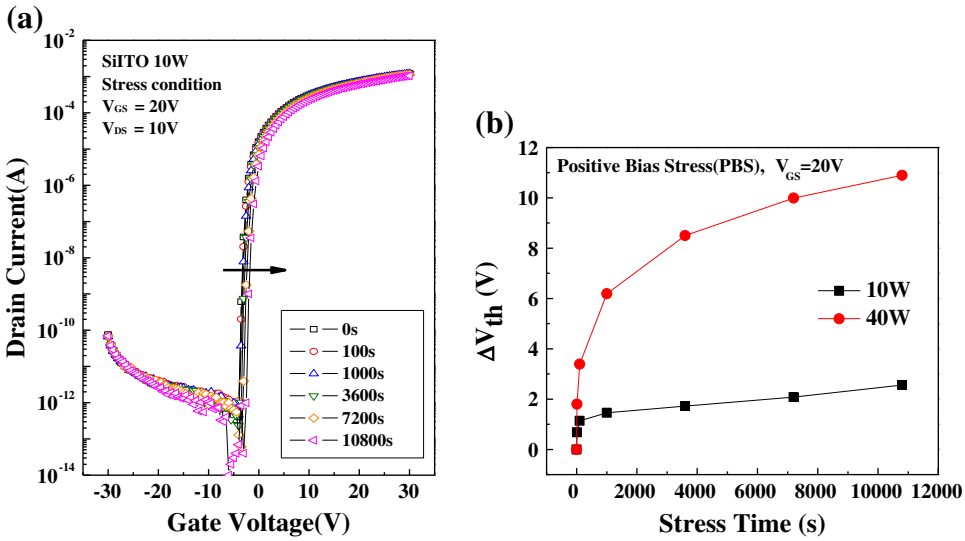

Fig. 3. (a) Evolution of transfer curve of TFT with *a*-SITO deposited at SiO_2 rf power of 10 W. (b) Threshold voltage shift (ΔV_{th}) under positive bias stress of *a*-SITO TFTs for different SiO_2 rf powers of 10 W and 40 W.

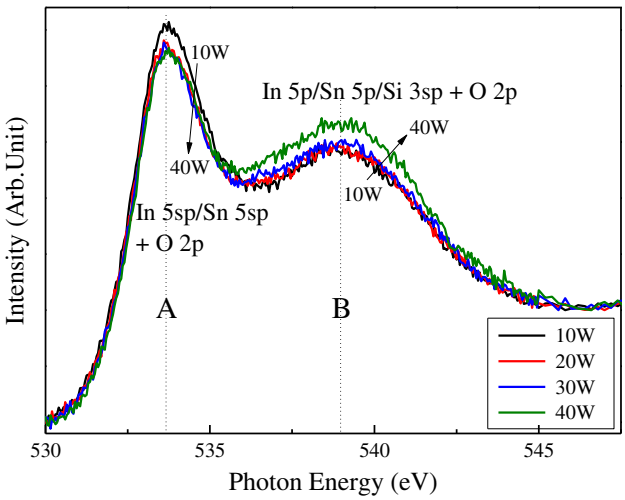

Fig. 4. O K-edge XAS spectra of *a*-SITO films as a function of SiO_2 rf power.

to 0.72 cm^2/Vs (4.22 at.% Si). In contrast, the V_{th} value gradually shifted in the positive direction with increasing silicon content. This can be attributed to decrease of the oxygen vacancies that act as shallow donor states due to the increase of strong Si–O bonds or increase of the total trap density in the *a*-SITO TFTs, resulting in a reduction of free electrons due to charge trapping in the dielectric/SITO channel layer.[19] Additionally, the output curves (I_{DS}–V_{DS} characteristics) showed a clear pinch-off and current saturation without current crowding in the low-V_{DS} region, which suggests that the SITO TFT operation is consistent with the standard field-effect transistor theory in Fig. 2c.

The bias instability of the TFTs with *a*-SITO active layers was also investigated as a function of the Si doping concentration under positive bias stress (PBS) condition (V_{GS} = +20 V, V_{DS} = +10 V), after 10 s, 100 s, 1000 s, 3600 s, 7200 s, and 10,800 s, as shown in Fig. 3a. With increasing stress time, the transfer characteristic of the *a*-SITO TFTs systematically shifted in the positive direction, without any significant change of the mobility or S.S. values. This suggests that the charge-trapping mechanism at the semiconductor–dielectric interface may be dominant in the bias instability of *a*-SITO TFTs.[20] As shown in Fig. 3b, the TFT with higher Si doping content shows a larger shift of the transfer curve in the positive direction. The V_{th} of the TFT with the *a*-SITO channel cosputtered at SiO_2 rf power of 40 W shifts by +10.9 V, while that deposited at 10 W exhibited a shift of only +2.56 V.

Next, the electronic structures related to the conduction band and the molecular orbital ordering of the *a*-SITO films were evaluated by XAS analysis. Figure 4 shows the normalized O K-edge spectra of *a*-SITO films as a function of the SiO_2 rf power. Normalization of the XAS spectra was carefully performed by subtracting an x-ray beam background from the raw data and subsequently scaling the difference between the pre- and post-edge levels, which can be used to compare qualitative changes of the conduction band and molecular orbital bonding symmetries.[21] The XAS spectra of SITO films could be mainly associated with the ITO.[22] The major features, denoted by "A" and "B," in the spectra of the *a*-SITO films can be attributed to the In 5*sp*/Sn 5*sp* + O 2*p* state and a composition of In 5*p*/Sn 5*p*/Si 3*sp* + O 2*p* states, respectively.[22–24] The qualitative changes, indicating a slight decrease in feature A and increase in feature B with increasing SiO_2 rf power, may reveal the decrease (increase) in In (Si) concentration in the *a*-SITO films. In other words, the changes of the conduction band mainly reflect

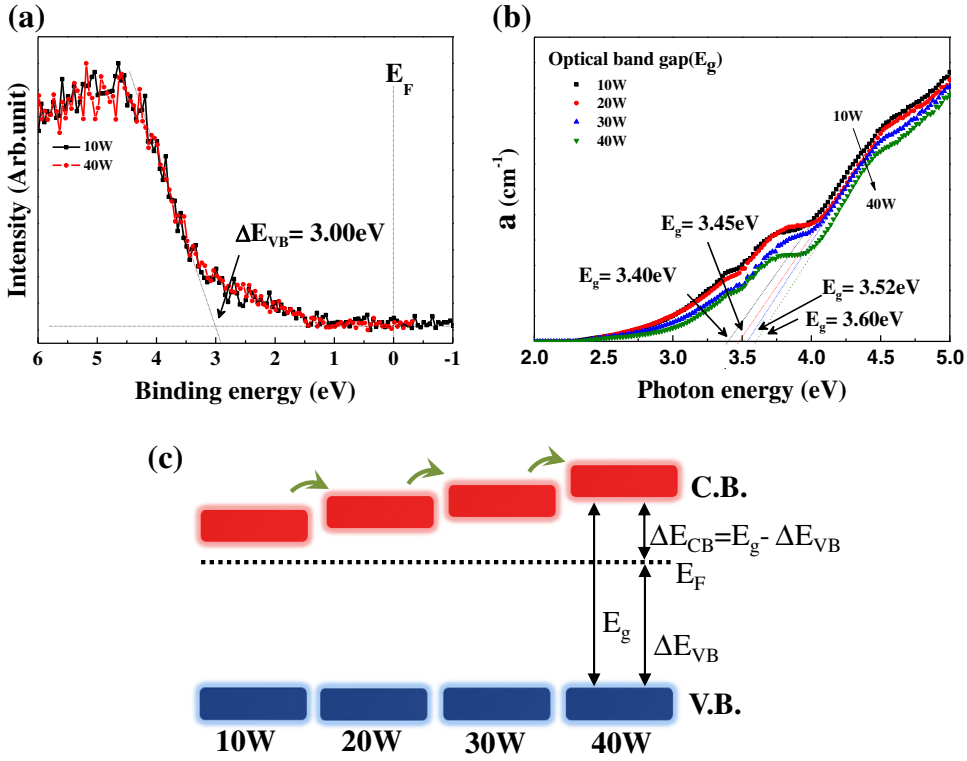

	Eg(eV)	ΔE_{VB}(eV)	ΔE_{CB}(eV)
10 W	**3.40 eV**	**3.30 eV**	**0.10 eV**
20 W	**3.45 eV**	**3.30 eV**	**0.15 eV**
30 W	**3.52 eV**	**3.30 eV**	**0.22 eV**
40 W	**3.60 eV**	**3.30 eV**	**0.30 eV**

Fig. 5. (a) XPS spectra near valence band, (b) imaginary dielectric function (ε_2) measured by SE, and (c) schematic energy level diagram reflecting the relative energy position of the Fermi level (E_F) with respect to the conduction-band minimum (C.B.) and valence band maximum (V.B.) as a function of the rf power applied to the SiO_2 target. The corresponding values of the bandgap (E_g) and the relative energy difference between E_F and V.B. (ΔE_{VB}) and between E_F and C.B. (ΔE_{CB}) are indicated below diagram (c).

the changes of the electronic structure due to the increase of the incorporated Si concentration in the a-SITO films.[23] Based on the XAS results, the most plausible dependence related to the electrical properties is the change of mobility, which exhibits a higher value with larger area in the region of the conduction-band minimum (feature A) and a lower value with an increase in molecular orbital structure (feature B) on incorporation of SiO_2.

To understand the detailed physical origin of the device characteristics of the a-SITO TFTs, we investigated the electronic structure of the a-SITO films, including the band alignment and band edge states below the conduction band. Figure 5a and b show the valence band spectra and bandgap (E_g) measured by XPS and SE using the extrapolation method. The values of E_g and the relative energy difference between the Fermi level (E_F) and valence-band maximum (ΔE_{VB}), and between E_F and the conduction-band minimum (ΔE_{CB}) are indicated below the diagram in Fig. 5c. The extracted valence-band offset (ΔE_{VB}) has the same value regardless of the applied SiO_2 rf power, while the extracted E_g increased from 3.40 eV to 3.60 eV with the increase of the SiO_2 rf power. As a result, the relative position of the Fermi level (ΔE_{CB}) shifts away from the conduction-band minimum by 0.10 eV (10 W) to 0.30 eV (40 W). This result would be related to the decrease of the carrier concentration (i.e., more positive V_{th}) with increasing Si concentration.[25]

Figure 6a shows the imaginary dielectric function (ε_2) spectra obtained from SE measurements for a-SITO film deposited at SiO_2 rf power of 40 W. These spectra were extracted from a simple four-phase model comprising a Si substrate, SiO_2 overlayer, a-SITO overlayer, and an ambient layer, as shown

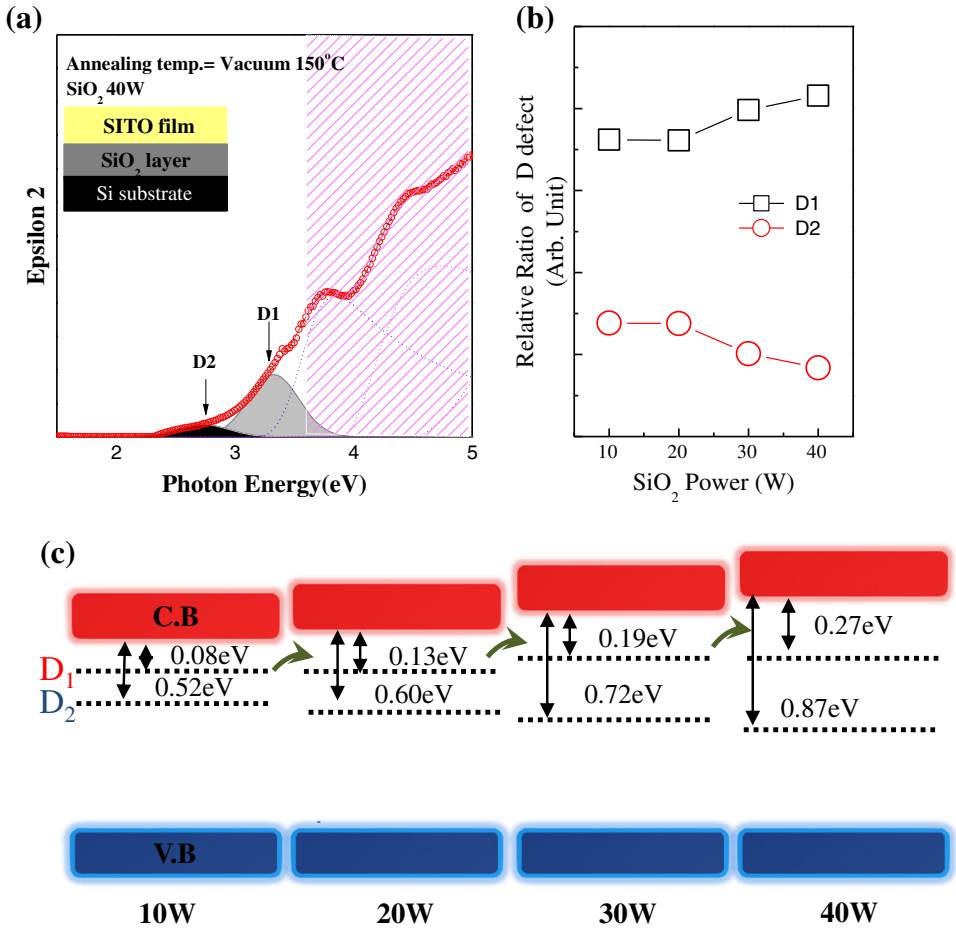

Fig. 6. (a) Imaginary dielectric function (ε_2) spectrum from SE measurements for *a*-SITO film deposited at SiO_2 rf power of 40 W. A distinct two deconvoluted peak, labeled as *D*1 and *D*2, is Gaussian fit and represents the band edge state located below the conduction-band edge. (b) Relative ratio of *D*1 peak as a function of the rf power applied to the SiO_2 target. (c) Schematic energy level diagrams reflecting the energy levels of the band edge states (*D*1 and *D*2) for different values of rf power applied to the SiO_2 target.

in the inset of Fig. 6a. A detailed and quantitative analysis of the band edge states and unoccupied states in the conduction band was performed by fitting using a Gaussian model (band edge states) and a Tauc–Lorentz model (conduction-band states).[26] A distinct two deconvoluted peak, labeled as shallow band edge state (*D*1) and deep band edge state (*D*2), represents the band edge state below the conduction-band edge. Considering the electrical data presented above, the variation of the *D*1 and *D*2 states can be correlated to the electrical properties, such as the carrier concentration and mobility, depending on the relative energy position within the bandgap.[27,28] Figure 6b shows the relative ratio of the band edge states (*D*1 and *D*2) in the SITO films as a function of the applied SiO_2 rf power. Based on the previous interpretation for ZnO film,[27] *a*-SITO film deposited at higher SiO_2 power (40 W) is considered to provide a larger carrier concentration and slightly greater mobility, because of the increase of the shallow (*D*1) and decrease of the deep (*D*2) band edge states, respectively. However, the results herein are conflicting, as the drastic decrease of the carrier concentration and mobility could be caused by the relative energy position from the conduction-band minimum. As shown in Fig. 6c, it is also noted that the relative energy positions of *D*1 and *D*2 shift to deeper levels from the conduction-band minimum with increase of the SiO_2 rf power (i.e., *D*1: 0.08 eV $\rightarrow$ 0.27 eV, *D*2: 0.52 eV $\rightarrow$ 0.87 eV), especially *D*2. Another interesting interpretation is associated with the deep band edge state (*D*2), which shifts to deeper energy position from the conduction-band minimum with increase of the SiO_2 rf power. This shift, along with the relative position of the Fermi level, may contribute to the degradation of mobility and stability, by charge trapping and increased charge scattering during carrier transport by the band edge states far from the conduction band.[27,28]

CONCLUSIONS

Si-doped ITO (SITO) thin films were developed by rf magnetron cosputtering of SiO_2 and ITO targets. The Si content in the SITO films was varied by

changing the SiO_2 rf power from 10 W to 40 W, whereas a constant power of 60 W was applied to the ITO target. The field-effect mobility and stability under PBS of the *a*-SITO TFTs with 0.22 at.% Si were significantly improved to 28.7 cm^2/Vs and 1.5 V shift of V_{th}, respectively, as compared with the values (0.72 cm^2/Vs and 8.9 V shift) for the *a*-SITO TFTs with 4.22 at.% Si. This suggests that the performance and stability of *a*-SITO TFTs are highly susceptible to variation of the Si concentration and thus that it is very important to fabricate *a*-SITO TFTs with optimized Si concentration for practical applications. It was found that *a*-SITO films deposited at low SiO_2 rf power of 10 W had smaller conduction-band offset, and the band edge states moved to deep energy levels from the conduction-band minimum with increasing applied SiO_2 rf power from 10 W to 40 W. It is suggested that these changes in the electronic structure could be the physical origin of the device performance and bias instability of *a*-SITO TFTs.

ACKNOWLEDGEMENTS

This research was partially supported by the Basic Science Research Program through the National Research Foundation of Korea (NRF), funded by the Ministry of Education, Science, and Technology (No. 2012011730 and NRF-2013R1A1A 2A10005186). This work was supported by the IT R&D program of MKE/KETI (Grant No. 10041416, The core technology development of light and space adaptable new mode display for energy saving on 7 in. and 2 W) and also by the Global Frontier R&D Program (2013-073298) of the Center for Hybrid Interface Materials (HIM) funded by the Ministry of Science, ICT, and Future Planning.

REFERENCES

1. K. Nomura, H. Ohta, A. Takagi, T. Kamiya, M. Hirano, and H. Hosono, *Nature* 432, 488 (2004).
2. J.S. Park, W.-J. Maeng, H.-S. Kim, and J.-S. Park, *Thin Solid Films* 520, 1679 (2012).
3. A. Walsh, J.F. da Silva, and S.H. Wei, *J. Phys.: Condens. Matter* 23, 334210 (2011).
4. J.H. Noh, S.Y. Ryu, S.J. Jo, C.S. Kim, S.-W. Sohn, P.D. Rack, D.-J. Kim, and H.K. Baik, *IEEE Electron Device Lett.* 31, 567 (2010).
5. W. Kim, J.-H. Bang, H.-S. Uhm, S.-H. Lee, and J.-S. Park, *Thin Solid Films* 519, 1573 (2010).
6. C.J. Chiu, S.P. Chang, and S.J. Chang, *IEEE Electron Device Lett.* 31, 1245 (2010).
7. M. Dai, G. Wu, Y. Yang, J. Jiang, L. Li, and Q. Wan, *Appl. Phys. Lett.* 98, 093506 (2010).
8. C.E. Kim and I. Yun, *Appl. Phys. Lett.* 100, 013501 (2012).
9. S.Y. Park, K.H. Ji, H.Y. Jung, J.-I. Kim, R. Choi, K.S. Son, M.K. Ryu, S. Lee, and J.K. Jeong, *Appl. Phys. Lett.* 100, 162108 (2012).
10. D.-H. Cho, S. Yang, C. Byun, J. Shin, M.K. Ryu, S.-H.K. Park, C.-S. Hwang, S.M. Chung, W.-S. Cheong, S.M. Yoon, and H.-Y. Chu, *Appl. Phys. Lett.* 93, 142111 (2008).
11. T. Iwasaki, N. Itagaki, T. Den, H. Kumomi, K. Nomura, T. Kamiya, and H. Hosono, *Appl. Phys. Lett.* 90, 242114 (2007).
12. C.-J. Kim, et al., *Appl. Phys. Lett.* 95, 252103 (2009).
13. J.-S. Park, K.-S. Kim, Y.-G. Park, Y.-G. Mo, H.D. Kim, and J.K. Jeong, *Adv. Mater.* 21, 329 (2009).
14. D.H. Kim, D.Y. Yoo, H.K. Jung, D.H. Kim, and S.Y. Lee, *Appl. Phys. Lett.* 99, 172106 (2011).
15. S. Tomai, M. Nishimura, M. Itose, M. Matuura, M. Kasami, S. Matsuzaki, H. Kawashima, F. Utsuno, and K. Yano, *Jpn. J. Appl. Phys.* 51, 03CB01 (2012).
16. S. Urakawa, S. Tomai, Y. Ueoka, H. Yamazaki, M. Kasami, K. Yano, D. Wang, M. Furuta, M. Horita, Y. Ishikawa, and Y. Uraoka, *Appl. Phys. Lett.* 102, 053506 (2013).
17. K.-H. Lim, K. Kim, S. Kim, S.Y. Park, H. Kim, and Y.S. Kim, *Adv. Mater.* 25, 2994 (2013).
18. J.H. Jeong, H.W. Yang, J.-S. Park, J.K. Jeong, Y.G. Mo, H.D. Kim, J.W. Song, and C.S. Hwang, *Electrochem. Solid-State Lett.* 11, 157 (2008).
19. S.Y. Lee, D.H. Kim, E. Chong, Y.W. Jeon, and D.H. Kim, *Appl. Phys. Lett.* 98, 122105 (2011).
20. R.B.M. Cross and M.M. De Souza, *Appl. Phys. Lett.* 89, 263513 (2006).
21. K.B. Chung, J.P. Long, H. Seo, G. Lucovsky, and D. Nordlund, *J. Appl. Phys.* 106, 074102 (2009).
22. C. McGuinness, C.B. Stagarescu, P.J. Ryan, J.E. Downes, D. Fu, and K.E. Smith, *Phys. Rev. B* 68, 165104 (2003).
23. H.-M. Lee, S.-B. Kang, K.-B. Chung, and H.-K. Kim, *Appl. Phys. Lett.* 102, 021914 (2013).
24. G. Lucovsky, D. Zeller, K. Wu, and J.L. Whitten, *Microelectron. Eng.* 88, 1537 (2011).
25. B.D. Ahn, J.H. Lim, M.-H. Cho, J.-S. Park, and K.-B. Chung, *J. Phys. D Appl. Phys.* 45, 415307 (2012).
26. D.E. Aspnes and A.A. Studna, *Phys. Rev. B* 27, 985 (1983).
27. H.-W. Park, J.-S. Park, J.H. Lee, and K.-B. Chung, *Electrochem. Solid-State Lett.* 15, H133 (2012).
28. H.-W. Park, B.-K. Kim, J.-S. Park, and K.-B. Chung, *Appl. Phys. Lett.* 102, 102102 (2013).